

Spatio-temporal patterns of Chaos in the Atlantic Overturning Circulation

Q. Jamet^{1*}, W. K. Dewar¹, N. Wienders¹ and B. Deremble²

¹Department of Earth, Ocean and Atmospheric Science, the Florida State University, Tallahassee, Florida

²Laboratoire de Météorologie Dynamique, Paris, France

Key Points:

- We highlight the existence of a basin scale intrinsic mode of AMOC variability sharing similarities with the atmospherically forced mode
- The RAPID-MOCHA-WBTS array is found to be part of this basin scale mode; 50% of its interannual variability is ascribed as intrinsic
- Our results provide an estimation of the quantitative accuracy of the overturning variability within eddy-resolving ocean models

*The Florida State University, 117 N Woodward Avenue, Tallahassee, FL 32306-4320.

Corresponding author: Quentin Jamet, qjamet@fsu.edu

Abstract

Examining an ensemble of high-resolution ($1/12^\circ$) North Atlantic ocean simulations, we provide new insights into the partitioning of the Atlantic Meridional Overturning Circulation (AMOC) variability between forced and intrinsic at low-frequency (2-30 years). We highlight the existence of a basin scale intrinsic mode that shares similarities with the atmospherically forced signal. The RAPID-MOCHA-WBTS array is found to be part of this mode, such that we ascribe 50% (~ 0.8 Sv) of its interannual variability as intrinsic. At decadal time scales, intrinsic variability is rather small (~ 0.2 Sv) compared to the recently observed 2-3 Sv AMOC downturn. This downturn is thus unlikely to be induced by locally generated intrinsic ocean dynamics. We interpret this intrinsic variability as 'chaotic', i.e. somewhat unpredictable, providing an estimation of the quantitative accuracy of AMOC variability within eddy-resolving numerical models.

1 Introduction

The Atlantic Meridional Overturning Circulation (AMOC) is an important oceanic component of the climate system, placing a premium on understanding its variability. It affects regional and global climate by modulating oceanic surface temperatures in the North Atlantic (Caesar et al., 2018; Knight et al., 2005; McCarthy et al., 2015), impacting precipitation over Europe (Sutton et al., 2012) and North Africa (Zhang et al., 2006) and influencing hurricane activity in North America (Goldenberg et al., 2001). The mechanisms driving AMOC variability remain however debated mostly due to the large spread in the simulated spatio-temporal patterns between models (Buckley et al., 2016), and due to the difficulties in validating numerical results against sparse and too short observational time series.

The atmosphere is thought to drive a significant portion of AMOC variability at various time scales, such that increasing greenhouse gases are expected to induce a decline of the AMOC (Caesar et al., 2018; Kirtman et al., 2013; Saba et al., 2016). Recent observations suggest that this decline is underway (Smeed et al., 2018). The link between the observed decline and the simulated response to increased greenhouse gases remains unclear however, with observed patterns of surface ocean metrics associated with the observed AMOC decline that resemble those found in climate models (Smeed et al., 2018), but with a much larger amplitude than the simulated long-term forced trend (Smeed et al., 2014). Aside from surface forcing, the ocean also develops its own intrinsic variabil-

45 ity (Penduff et al., 2011; Sérazin et al., 2015), so the AMOC strength does not only
46 depend on the atmosphere. The contribution of such intrinsically driven ocean dynamics
47 for the low-frequency AMOC variability has been recently underscored (Grégorio et al.,
48 2015; Leroux et al., 2018), but our understanding of such processes is rather limited. This
49 study sheds more light on such a contribution, and discuss implications for the interpre-
50 tation of observational data set such as the RAPID-MOCHA-WBTS program.

51 To describe this variability, we use here an ensemble of numerical simulations of
52 the North Atlantic. As we shall see, we tailored this ensemble to separate the AMOC
53 variability into two contributions: The intrinsic (locally generated) variability and the
54 atmospherically forced variability. We use a high resolution ($1/12^\circ$), regional (20°S to
55 55°N) North Atlantic configuration to produce a 12-member ensemble consisting of 50-
56 year long members, spanning the period 1963-2012. Each ensemble member corresponds
57 to the same model configuration (external forcing and open boundary conditions). The
58 only difference between the members of the ensemble is the initial condition. We pro-
59 vide a full description of the model in Section 2. In Section 3, we quantify the contri-
60 bution of the internal ocean dynamics for the total low-frequency AMOC variability, and
61 highlight the existence of a basin scale mode of intrinsic low-frequency AMOC variabil-
62 ity. We propose a link between these results and observations at 26.5°N provided by the
63 RAPID-MOCHA-WBTS program (McCarthy et al., 2015) in Section 4. We conclude and
64 discuss the results in Section 5.

65 **2 Model and Methods**

66 The 12-members ensemble simulation is performed with a regional configuration
67 of the Massachusetts Institute of Technology General Circulation Model (MITgcm, Mar-
68 shall et al., 1997). The North Atlantic domain extends from 20°S to 55°N . The horizon-
69 tal resolution is $1/12^\circ$ and we have 46 layers on the vertical ranging from 6 m at the sur-
70 face to 250 m at depth. Water masses that enter or leave the domain through the north-
71 ern and the southern boundaries of the domain, as well as at the Strait of Gibraltar, are
72 represented through the use of open boundary conditions derived from the 55-year long
73 $1/12^\circ$ horizontal resolution ocean-only global configuration ORCA12.L46-MJM88 (Mo-
74 lines et al., 2014; Sérazin et al., 2015), spatially interpolated on our model grid. At the
75 surface, the ocean model is coupled to an atmospheric boundary layer model (Cheap-
76 AML, Deremble et al., 2013). This approach is used to better represent air-sea exchanges,

77 and to avoid the suppression of surface ocean dynamics caused by a prescribed atmo-
 78 sphere with an infinite heat capacity. The configuration is integrated forward in time for
 79 50 years over the period 1963-2012 with a 12-members ensemble strategy. Further de-
 80 tails on the configuration, the initial conditions, and the simulated North Atlantic oceanic
 81 mean state are given in Supporting Information.

82 To assess low-frequency intrinsic AMOC variability, we first remove trends and fre-
 83 quencies lower than 50 years in each ensemble member, estimated with a nonparamet-
 84 ric locally estimated scatterplot smoothing (LOESS, Cleveland et al., 1988) operator.
 85 We compute a climatological annual cycle from the 50-year ensemble mean, and then re-
 86 move this annual cycle from each member. Finally, the residuals are low-pass filtered with
 87 a 1-year cut-off period to remove the overwhelmingly large, daily to weekly variability
 88 due to atmospheric forcing. This filtering procedure isolates the ocean variability in the
 89 2 to 30 year time bands (cf. Supporting Information).

90 We use a statistical approach to separate the intrinsically generated from the ex-
 91 ternally forced variabilities in our ensemble. We first compute an ensemble mean (50 years
 92 long time series) by averaging the oceanic state simulated by the 12 members. This time
 93 series represents the signal that is common to all members, and is assumed to originate
 94 from the external forcing, either from the surface or through the open boundaries. We
 95 interpret the ensemble mean as the forced signal, and define its temporal variance σ_F^2
 96 following Leroux et al. (2018):

$$\sigma_F^2 = \frac{1}{T-1} \sum_{t=1}^T \left[\langle f_i(t) \rangle - \overline{\langle f_i(t) \rangle} \right]^2, \quad (1)$$

97 with T the length of the 50-year long simulations, $\langle . \rangle$ the ensemble mean operator
 98 and \bar{x} the time mean operator. Since only initial conditions differ between each realiza-
 99 tion, the residual of each member with respect to the ensemble mean is, by construction,
 100 due to ocean dynamics sensitive to the initial conditions. We interpreted this residual
 101 signal as the intrinsic variability, and define its variance σ_I^2 following Leroux et al. (2018):

$$\sigma_I^2 = \frac{1}{N-1} \sum_{i=1}^N [f_i(t) - \langle f_i(t) \rangle]^2, \quad (2)$$

102 with $N = 12$ the number of members, $i = 1, \dots, N$ the member number. The total vari-
 103 ance is simply defined as the sum of the intrinsic and the forced variance $\sigma_T^2 = \sigma_I^2 +$
 104 σ_F^2 .

3 The intrinsic AMOC variability

We plot in Fig. 1 the intrinsic-to-total AMOC variance ratio $R = \frac{\sigma_I^2}{\sigma_T^2}$ in latitude-depth space. This provides a measure of the relative contribution of ocean internal dynamics for the total AMOC variance at interannual-to-decadal time scales. Intrinsic AMOC variability is routinely 50%, and exceeds 60% in the deep North Atlantic. Surface ratios are typically smaller, reflecting an increasing control of the AMOC by the atmosphere, although ratios of 30% are common. R exceeds 50% at 400 meters near 38°N where the Gulf Stream separates from the east coast of the United States, highlighting the strong meso-scale contribution to AMOC variability. Our estimates of the intrinsic-to-total ratio are somewhat larger than earlier studies for this region, but those were conducted with either a different method (Grégorio et al., 2015), or at coarser resolution (Leroux et al., 2018). At 26.5°N, R exceeds 40% as shallow as 500 meters, and increases near the bottom. Intrinsically driven versus forced AMOC variability at that location is further discussed in Section 4.

We now wish to extract the leading modes of forced and intrinsic AMOC variability in the latitude-depth space and compare their respective spatio-temporal patterns. We plot the first Empirical Orthogonal Function (EOF) of the ensemble mean AMOC on the top left panel of Fig. 2. It explains roughly 40% of the total forced AMOC variance, and is characterized by a broad positive signal from about 10°S to roughly 45°N, and negative signal elsewhere. The change of sign around 45°N is associated with a change of sign in the first EOF of the zonal winds (not shown). This pattern strongly resembles the delayed response of the AMOC to the North Atlantic Oscillation (NAO) usually identified in climate and ocean models (Deshayes et al., 2008; Eden et al., 2001; Gastineau et al., 2012). Furthermore, its associated Principal Component (PC, bottom left panel) peaks in the 2-3 and 6-8 year frequency bands typical of the NAO spectrum (Czaja et al., 2001; Reintges et al., 2017). We thus interpret this first EOF as the signature of a local, atmospherically forced AMOC variability.

To extract the leading mode of intrinsic AMOC variability, we perform a Principal Component Analyses for each ensemble residual and average the results (Fig. 2). We first note that the 10 first EOFs explain about 75% of the total intrinsic AMOC variance, while this number reaches more than 90% in the case of the forced signal. Such difference is indicative of a less organized intrinsic variability. The variance explained

137 by the first intrinsic EOF is relatively high ($\sim 30\%$), and the averaging procedure high-
138 lights the emergence of a large scale mode of variability extending from 10°S to about
139 35°N with a maximum of about 1 Sv ($1\text{ Sv} = 10^6\text{ m}^3\text{s}^{-1}$) around 20°N and 2000 m depth.
140 This pattern exhibits spatial similarities with the atmospherically forced mode discussed
141 earlier. Notable differences arise however in their spectral properties, where both intrinsic
142 and forced leading modes peak (locally) at interannual time scales. The intrinsic PSD
143 decreases monotonically at lower frequencies whereas the forced mode dominates at long
144 time scales. This suggest that in the future generation of climate models with eddy re-
145 solving ocean models, projections of future changes in the North Atlantic overturning
146 would be somewhat limited at interannual timescales, but might benefit of better pre-
147 dictive skills at decadal and longer timescales.

148 Finally, note that, although intrinsic variability controls more than 50% of the to-
149 tal variability in the Gulf Stream (Fig. 1), this region does not appear to be part of the
150 leading mode of intrinsic AMOC variability. We suspect this is due to the mesoscale dy-
151 namics of this region, and Gulf Stream instabilities. As a result, although some signal
152 are found in the second (Fig. S7) and subsequent EOFs for each individual member, they
153 take place at slightly different locations such that averaging strongly damp their signa-
154 ture (Fig. 2, middle right panel). In other word, such modes of variability are member-
155 dependent, and not considered here.

156 **4 A focus on RAPID observations**

157 We now wish to replace our ensemble-based results in the context of observations
158 and discuss implications for the interpretation of observational data set. The RAPID-
159 MOCHA-WBTS program (McCarthy et al., 2015) refers to a large, multi-national ef-
160 fort to monitor the strength of the AMOC, principally at 26.5°N in the North Atlantic.
161 We have computed numerical equivalents of the observed AMOC by integrating net model
162 northward transport across the North Atlantic, from Florida to the east coast of Africa
163 (cf Supporting Information). Left panel of Fig. 3 compares the time evolution of the AMOC
164 northward transport anomalies at 1200 meters, the maximum AMOC (Fig. 1), as mea-
165 sured by the RAPID array (red line) against that simulated by our 12 ensemble mem-
166 bers (thin gray lines). We first note that our simulated AMOCs tend to underestimate
167 the observations at the beginning of the record and overestimate them toward the end.
168 This mismatch is associated with the observed weakening (2-3 Sv) AMOC trend from

169 2004 to 2012, a decrease argued to be due to a change in mid-ocean geostrophic (Smeed
170 et al., 2014). Our simulations do not capture this over the 2005-2011 timeframe, and we
171 do not either obtain intrinsic low-frequency variability this large. The PSD of the sec-
172 ond intrinsic mode of variability is found to dominate over the forced component at decadal
173 time scale (Fig. 2, bottom right panel). However, this second EOF explains only 10%
174 of the intrinsic variance, such that it is likely to contribute only for ~ 0.2 Sv to the to-
175 tal AMOC variability. We thus conclude that the observed 2-3 Sv AMOC transport down-
176 turn between 2004 and 2012 cannot be explained as local intrinsic variability only. We
177 have conducted additional sensitivity experiments on the choice of open boundary con-
178 ditions (not shown), and found that decadal AMOC variability at 26.5°N are mostly driven
179 by remote signals. Further investigations of such remote signals in our North Atlantic
180 regional configuration are underway and will be reported somewhere else.

181 The level of agreement between the observed and ensemble mean AMOC transports
182 (Fig. 3, black line) remains however fairly high (correlation $r = 0.8$), with predominant
183 near-seasonal fluctuations of $\sim O(1)$ Sv). The pronounced weakening (~ 3 Sv) of the AMOC
184 over the period 2009/2010 interpreted by others as due to atmospheric forcing (Roberts
185 et al., 2013) is for instance well reproduced by all members. Each exhibits peculiarities
186 however, such that AMOC variability is also member-dependent, highlighting the pres-
187 ence of an intrinsic variability at that location. At 26.5°N , our estimate of the intrinsic-
188 to-total variance ratio R exceeds 40% at 1200 meters, the maximum AMOC (Fig. 1). The
189 power spectral analysis of the simulated time series (Fig. 3, right panel) reveals that in-
190 trinsic ocean dynamics contributes about 50% at interannual time scales and about 20-
191 25% at decadal time scales. In terms of volume transport, these variabilities are asso-
192 ciated with an AMOC standard deviation of about 0.8 Sv and 0.2 Sv, respectively. This
193 time scale separation between forced and intrinsic variability echoes the differences in
194 spectral properties between the leading modes of forced and intrinsic AMOC variabil-
195 ity discussed earlier (Section 3).

196 To shed light on such a potential connection between the temporal variability at
197 26.5°N and the leading mode of AMOC variability, we have regressed the AMOC sig-
198 nals in the latitude-depth space onto the the time series at 26.5°N (Fig. 4). The forced
199 ocean response at the RAPID location is associated with positively correlated anoma-
200 lies from 10°S to 45°N intensified between 1000 and 2000 meters, and negatively corre-
201 lated anomalies elsewhere. This spatial pattern strongly resembles the first EOF of the

202 forced signal (Fig. 2), with a correlation factor of $r = 0.81$ between associated time se-
203 ries. Similarly, the regression pattern for the intrinsic AMOC variability at 26.5°N re-
204 sembles the first EOF of the intrinsic signal (Fig. 2), with positively correlated anoma-
205 lies from 10°S to about 35°N (Fig. 4, right panel), and a correlation factor of $r = 0.68$
206 between associated time series. The similarities between regression maps and EOFs strongly
207 suggest that the temporal variability at 26.5°N is part of a spatially distributed North
208 Atlantic structure, with both intrinsic and forced origins that mostly differ by their spec-
209 tral properties.

210 5 Conclusion

211 We have discussed here the results of an ensemble-based examination of the At-
212 lantic Meridional Overturning Circulation (AMOC) variability at low-frequency (2-30
213 years) and we have identified the dominant spatio-temporal patterns of variability when
214 mesoscale ocean eddies are resolved. Our results suggest that a significant fraction of the
215 AMOC variability is sensitive to initial conditions, or in other words, is 'chaotic'. The
216 contribution of such a chaos is found to exceed 50% in the Gulf Stream region, and to
217 40-50% at the RAPID location. By extracting the leading modes of variability through
218 Principal Component Analysis, we have revealed the presence of a basin scale mode of
219 intrinsic AMOC variability in the North Atlantic. The variability of this intrinsic mode
220 peaks at interannual time scales, and its spatial pattern resemble the mode of AMOC
221 variability locally forced by the atmosphere. These results extend in the latitude-depth
222 space earlier investigations of intrinsically versus forced AMOC variability performed by
223 Grégorio et al. (2015) and Leroux et al. (2018) for a given depth.

224 We also compared our model output with the RAPID-MOCHA-WBTS program
225 for which continuous measurements of the AMOC at 26.5°N are performed since 2004
226 (McCarthy et al., 2015). At low-frequency, the dominant observed trend in the left panel
227 of Fig. 3 is the 2-3 Sv AMOC transport downturn interpreted by Smeed et al. (2014)
228 as a result of mid-ocean geostrophic dynamics. Our simulations do not capture this over
229 the 2005-2011 timeframe. Moreover, we do not obtain intrinsic low-frequency variabil-
230 ity this large; our low-frequency fluctuation estimates are more like ~ 0.2 Sv. The ob-
231 served downturn can thus not be attributed to local intrinsic variability only, although
232 our estimate remains in the range of long-term AMOC forced trends simulated by cli-
233 mate models (Caesar et al., 2018). However, we also emphasize our results are limited

234 to intrinsic variability of North Atlantic origin. We focus here on one ensemble, but have
235 others where boundary conditions are varying. Their analyses, not detailed here, sug-
236 gest the downturn originates perhaps in the Labrador (Jackson et al., 2016) or Nordic
237 Seas, with an unknown forced or intrinsic origin.

238 The simulated and observed signals agree fairly well in the high frequency band,
239 where predominant AMOC variations of $\sim O(1 \text{ Sv})$ of the observed signal are consistently
240 captured by the ensemble mean. We have found the leading forced EOF peaks at 2-3
241 years, and interpret this as atmospherically forced AMOC interannual variability. This
242 is consistent with the previous interpretation of the 2009-2010 event as atmospherically
243 forced (Roberts et al., 2013). We note that all members are not phase locked to the at-
244 mosphere because of the intrinsic dynamic of the ocean, with a contribution ($\sigma_I^{HF} = 0.8 \text{ Sv}$)
245 that equals the forced signal at interannual time scales. Equivalently, a significant frac-
246 tion of the interannual AMOC variability at 26.5°N is chaotic, and thus the RAPID time-
247 series represents only one possible trajectory among many. At interannual time scales,
248 roughly half of the expected variability cannot be predicted in advance. These results
249 provide a first estimate of the quantitative accuracy of the AMOC within numerical mod-
250 els. Probabilistic estimates as in Chapron et al. (2018) might well represent a useful av-
251 enue for further pursuit.

252 **Acknowledgments**

253 This work has been funded by the NSF award OCE1537304. It is a contribution to the
254 international CHAOCEAN program. Highperformance computing resources on Cheyenne
255 (doi:10.5065/D6RX99HX) have been provided by NCAR's Computational and Informa-
256 tion Systems Laboratory, sponsored by the National Science Foundation, under the uni-
257 versity large allocations UFSU0011. We also acknowledge Bernard Barnier from l'Institut
258 des Goscience de l'Environnement (IGE, Grenoble, France) and his collaborators for pro-
259 viding us all necessary data to force our regional model. Data used in this study are avail-
260 able at http://ocean.fsu.edu/~qjamet/share/data/chaos_amoc_GRL2019/.

261 **References**

262 Buckley, M. W., & Marshall, J. (2016). Observations, inferences, and mechanisms
263 of the Atlantic Meridional Overturning Circulation: A review. *Reviews of Geo-*
264 *physics*, *54*(1), 5–63.

- 265 Caesar, L., Rahmstorf, S., Robinson, A., Feulner, G., & Saba, V. (2018). Observed
 266 fingerprint of a weakening Atlantic Ocean overturning circulation. *Nature*,
 267 *556*(7700), 191.
- 268 Chapron, B., Dérian, P., Mémin, E., & Resseguier, V. (2018). Large-scale flows un-
 269 der location uncertainty: a consistent stochastic framework. *Quarterly Journal*
 270 *of the Royal Meteorological Society*, *144*(710), 251–260.
- 271 Cleveland, W. S., & Devlin, S. J. (1988). Locally weighted regression: an approach
 272 to regression analysis by local fitting. *Journal of the American statistical asso-*
 273 *ciation*, *83*(403), 596–610.
- 274 Czaja, A., & Marshall, J. (2001). Observations of atmosphere-ocean coupling in
 275 the North Atlantic. *Quarterly Journal of the Royal Meteorological Society*,
 276 *127*(576), 1893–1916.
- 277 Deremble, B., Wienders, N., & Dewar, W. (2013). Cheapaml: A simple, atmo-
 278 spheric boundary layer model for use in ocean-only model calculations. *Mon.*
 279 *Wea. Rev.*, *141*(2), 809–821.
- 280 Deser, C., Phillips, A., Bourdette, V., & Teng, H. (2012). Uncertainty in climate
 281 change projections: the role of internal variability. *Climate dynamics*, *38*(3-4),
 282 527–546.
- 283 Deshayes, J., & Frankignoul, C. (2008). Simulated variability of the circulation in
 284 the North Atlantic from 1953 to 2003. *J. Clim.*, *21*(19), 4919–4933.
- 285 Eden, C., & Jung, T. (2001). North Atlantic interdecadal variability: Oceanic re-
 286 sponse to the North Atlantic Oscillation (1865-1997). *J. Clim.*, *14*, 676-691.
- 287 Gastineau, G., & Frankignoul, C. (2012). Cold-season atmospheric response to
 288 the natural variability of the Atlantic meridional overturning circulation. *Clim.*
 289 *Dyn.*, *39*(1-2), 37–57.
- 290 Germe, A., Sévellec, F., Mignot, J., Swingedouw, D., & Nguyen, S. (2017). On the
 291 robustness of near term climate predictability regarding initial state uncertain-
 292 ties. *Climate dynamics*, *48*(1-2), 353–366.
- 293 Goldenberg, S. B., Landsea, C. W., Mestas-Nuñez, A. M., & Gray, W. M. (2001).
 294 The recent increase in atlantic hurricane activity: Causes and implications.
 295 *Science*, *293*(5529), 474–479.
- 296 Grégorio, S., Penduff, T., Sérazin, G., Molines, J.-M., Barnier, B., & Hirschi, J.
 297 (2015). Intrinsic variability of the atlantic meridional overturning circulation

- 298 at interannual-to-multidecadal time scales. *Journal of Physical Oceanography*,
 299 *45*(7), 1929–1946.
- 300 Jackson, L. C., Peterson, K. A., Roberts, C. D., & Wood, R. A. (2016). Recent slow-
 301 ing of Atlantic overturning circulation as a recovery from earlier strengthening.
 302 *Nature Geoscience*, *9*(7), 518.
- 303 Kirtman, B., Power, S., Adedoyin, A., Boer, G., Bojariu, R., Camilloni, I., . . . others
 304 (2013). Near-term climate change: projections and predictability.
- 305 Knight, J. R., Allan, R. J., Folland, C. K., Vellinga, M., & Mann, M. E. (2005).
 306 A signature of persistent natural thermohaline circulation cycles in observed
 307 climate. *Geophys. Res. Lett.*, *32*(L20708).
- 308 Leroux, S., Penduff, T., Bessières, L., Molines, J.-M., Brankart, J.-M., Sérazin, G.,
 309 . . . Terray, L. (2018). Intrinsic and Atmospherically Forced Variability of the
 310 AMOC: Insights from a Large-Ensemble Ocean Hindcast. *Journal of Climate*,
 311 *31*(3), 1183–1203.
- 312 Lorenz, E. N. (1963). Deterministic nonperiodic flow. *Journal of the atmospheric*
 313 *sciences*, *20*(2), 130–141.
- 314 Marshall, J., Adcroft, A., Hill, C., Perelman, L., & Heisey, C. (1997). A finite-
 315 volume, incompressible Navier Stokes model for studies of the ocean on parallel
 316 computers. *J. Geophys. Res.*, *102*(C3), 5753–5766.
- 317 McCarthy, G.D., Smeed, D.A., Johns, W.E., Frajka-Williams, E., Moat, B.I.,
 318 Rayner, D., Baringer, M.O., Meinen, C.S., Collins, J., . . . Bryden, H.L. (2015).
 319 Measuring the atlantic meridional overturning circulation at 26 n. *Progress in*
 320 *Oceanography*, *130*, 91–111.
- 321 McCarthy, G. D., Haigh, I. D., Hirschi, J. J.-M., Grist, J. P., & Smeed, D. A.
 322 (2015). Ocean impact on decadal Atlantic climate variability revealed by
 323 sea-level observations. *Nature*, *521*(7553), 508–510.
- 324 Molines, J., Barnier, B., Penduff, T., Treguier, A., & Le Sommer, J. (2014).
 325 *Orca12. l46 climatological and interannual simulations forced with dfs4. 4:*
 326 *Gjm02 and mjm88. drakkar group experiment rep* (Tech. Rep.). GDRI-
 327 DRAKKAR-2014-03-19, 50 pp.[Available online at [http://www.drakkar-ocean.](http://www.drakkar-ocean.eu/publications/reports/orca12_reference_experiments_2014)
 328 [eu/publications/reports/orca12_reference_experiments_2014](http://www.drakkar-ocean.eu/publications/reports/orca12_reference_experiments_2014).]
- 329 Penduff, T., Juza, M., Barnier, B., Zika, J., Dewar, W. K., Treguier, A.-M., . . . Aud-
 330 iffren, N. (2011). Sea level expression of intrinsic and forced ocean variabilities

- 331 at interannual time scales. *J. Clim.*, *24*(21), 5652–5670.
- 332 Reintges, A., Latif, M., & Park, W. (2017). Sub-decadal North Atlantic Oscilla-
333 tion variability in observations and the Kiel climate model. *Climate Dynamics*,
334 *48*(11-12), 3475–3487.
- 335 Roberts, C., Waters, J., Peterson, K., Palmer, M., McCarthy, G., Frajka-Williams,
336 E., ... others (2013). Atmosphere drives recent interannual variability of the
337 Atlantic meridional overturning circulation at 26.5 N. *Geophysical Research*
338 *Letters*, *40*(19), 5164–5170.
- 339 Saba, V. S., Griffies, S. M., Anderson, W. G., Winton, M., Alexander, M. A., Del-
340 worth, T. L., ... others (2016). Enhanced warming of the Northwest At-
341 lantic Ocean under climate change. *Journal of Geophysical Research: Oceans*,
342 *121*(1), 118–132.
- 343 Sérazin, G., Penduff, T., Grégorio, S., Barnier, B., Molines, J.-M., & Terray, L.
344 (2015). Intrinsic variability of sea level from global ocean simulations: Spa-
345 tiotemporal scales. *J. Clim.*, *28*(10), 4279–4292.
- 346 Smeed, D., Josey, S., Beaulieu, C., Johns, W., Moat, B., Frajka-Williams, E., ...
347 others (2018). The North Atlantic Ocean is in a state of reduced overturning.
348 *Geophysical Research Letters*, *45*(3), 1527–1533.
- 349 Smeed, D., McCarthy, G., Cunningham, S., Frajka-Williams, E., Rayner, D., Johns,
350 W., ... others (2014). Observed decline of the atlantic meridional overturning
351 circulation 2004–2012. *Ocean Science*, *10*(1), 29–38.
- 352 Sutton, R. T., & Dong, B. (2012). Atlantic Ocean influence on a shift in European
353 climate in the 1990s. *Nature Geoscience*, *5*(11), 788.
- 354 Zhang, R., & Delworth, T. L. (2006). Impact of Atlantic multidecadal oscillations
355 on India/Sahel rainfall and Atlantic hurricanes. *Geophysical Research Letters*,
356 *33*(17).

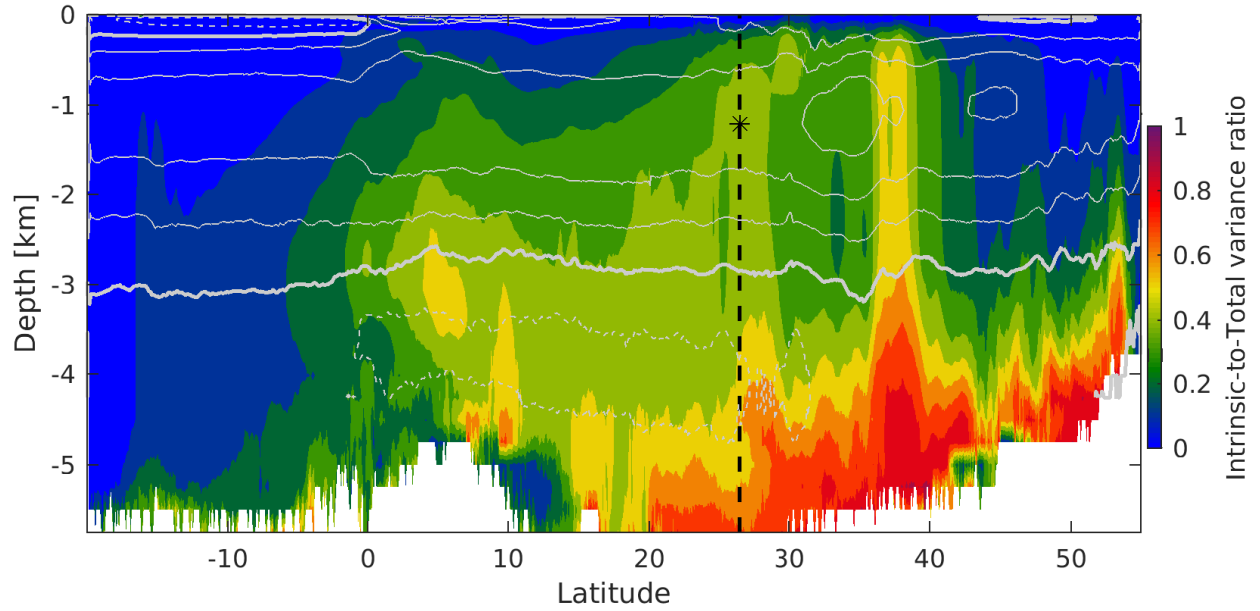


Figure 1. Intrinsic-to-total variance ratio $R = \frac{\sigma_I^2}{\sigma_T^2}$ of the simulated interannual-to-decadal AMOC variability. R indicates the fraction of the low-frequency AMOC variability that is driven by the chaotic internal ocean dynamics in the ensemble simulation (color contours every 0.1). Gray contours indicate the simulated time mean AMOC, with a contour interval of 5 Sv (1 Sv = $10^6 \text{ m}^3\text{s}^{-1}$) and a thick contour for zero values. The black dashed line represents the location of the RAPID array at 26.5°N , and the black star indicates the depth of 1200 m used in Fig. 3.

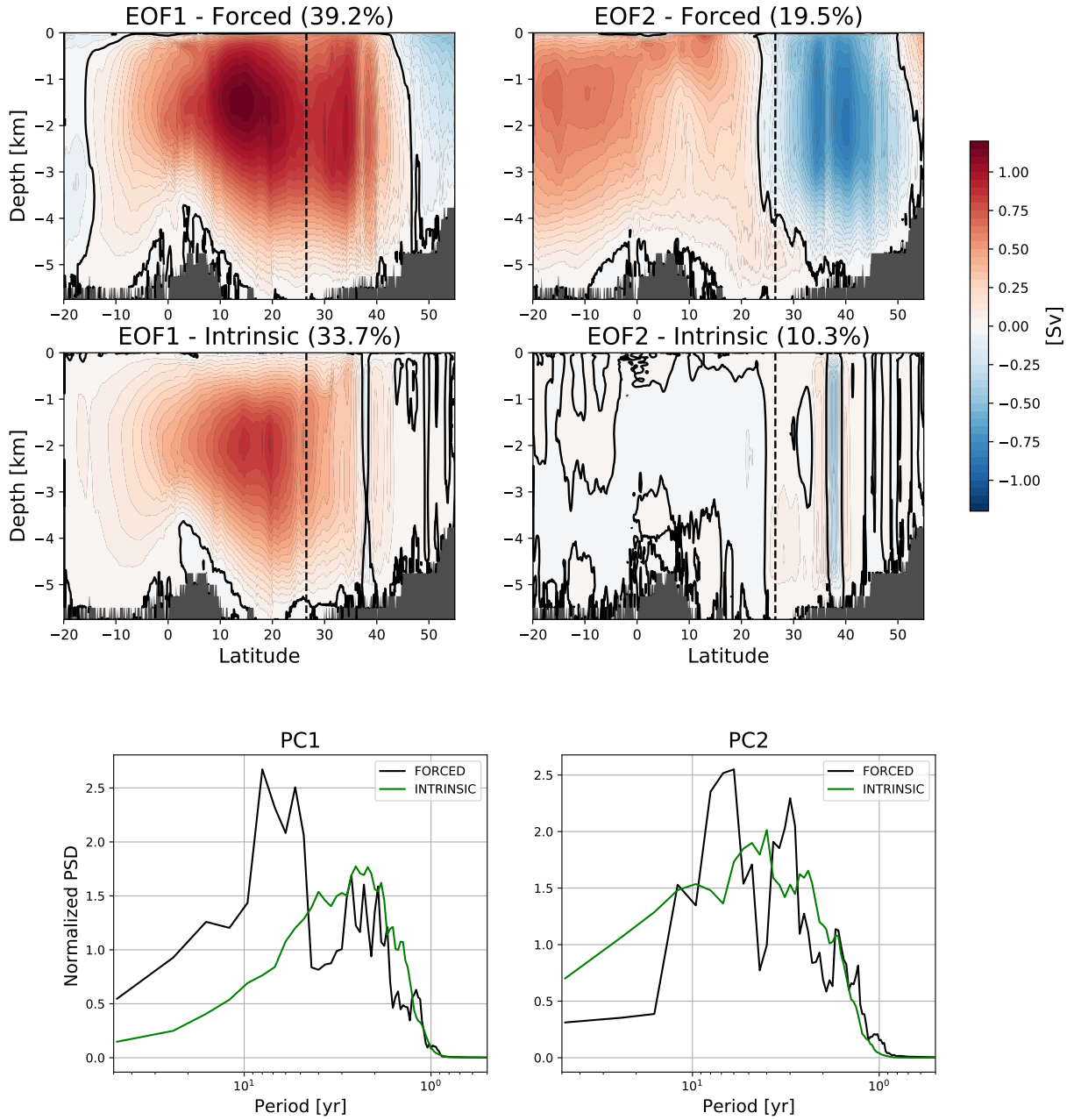


Figure 2. First (left) and second (right) Empirical Orthogonal Functions (EOFs) for the ensemble mean AMOC (top), for the intrinsic AMOC variability (middle), and the Power Spectral Density (PSD) function of the associated Principal Component (PC, bottom). The EOFs have been normalized such that they contain the amplitude in Sv of the explained signal, and the explained variance is shown on top of each panel. For the intrinsic component, the EOF and associated spectra have been computed for each individual member and then averaged together.

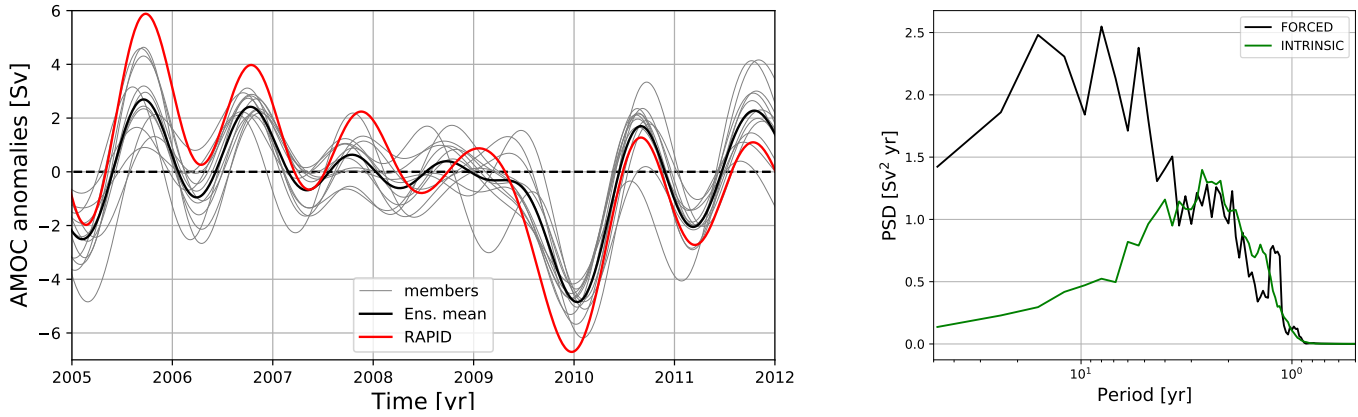


Figure 3. (Left) Time series corresponding to the variations of the northward AMOC transport, the maximum of which occurs around 1200 m depth in our model. Individual ensemble members are in light gray and the ensemble mean in black. The measured AMOC at the same depth appears in red. All data have been low-pass filtered with a cutoff at 1 year. The first and last years of data have been discarded due to side effects induced by the filter. (Right) Power Spectral Density (PSD) of the forced (black) and intrinsic (green) component of the simulated AMOC anomalies at 26.5°N and 1200 m for the 50-yr long signal. Data have been high-pass filtered and a seasonal cycle has been removed before the application of the 1-yr low-pass filter (see text for details). First and last years have been discarded due to side effects induced by the filter.

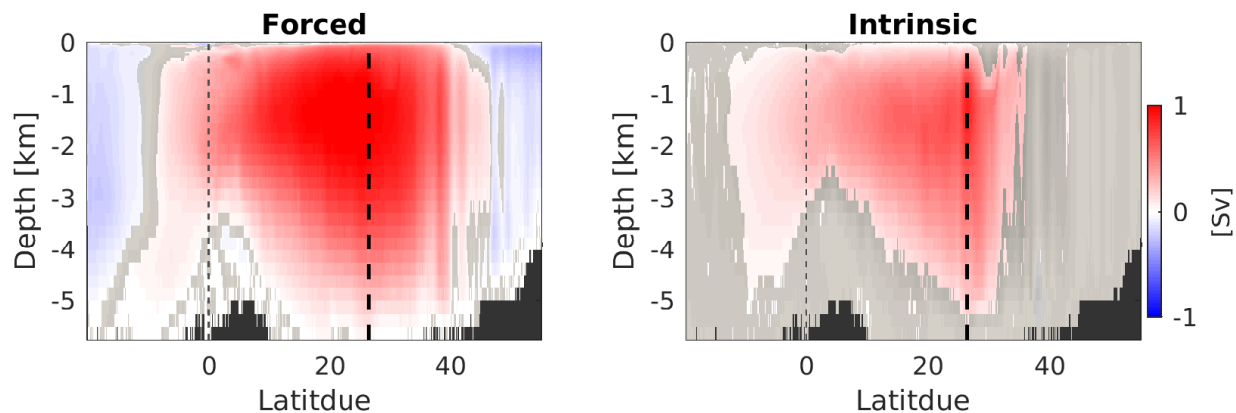


Figure 4. Regressed AMOC [Sv] in the latitude-depth space onto the AMOC time series at 26.5°N and 1200 m for the forced (left) and the intrinsic (right) component. Statistical significance has been assessed with a Monte Carlo approach by comparing the regression to that of a randomly scrambled ensemble. We have randomly permuted the AMOC time series by block of 15 days and compute a regression. This process, which aims at removing autocorrelation in the time series, is repeated 100 times. If the original regression is larger than 95% of the scrambled ensemble regressions, it is considered as statistically significant. Regressions that are not statistically significant are gray shaded. The black dashed line represents the location of the RAPID array at 26.5°N .